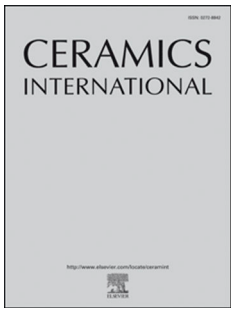

Low-temperature thermally modified fir-derived biomorphic C–SiC composites prepared by sol-gel infiltration

Guo-Qing Li, Min Yu, Hang Luo, Ze-Ya Huang, Ren-Li Fu, Francesco Gucci, Theo Saunders, Kong-Jun Zhu, Dou Zhang

PII: S0272-8842(22)04141-4

DOI: https://doi.org/10.1016/j.ceramint.2022.11.119

Reference: CERI 34926

To appear in: *Ceramics International*

Received Date: 2 August 2022

Revised Date: 21 October 2022

Accepted Date: 8 November 2022

Please cite this article as: G.-Q. Li, M. Yu, H. Luo, Z.-Y. Huang, R.-L. Fu, F. Gucci, T. Saunders, K.-J. Zhu, D. Zhang, Low-temperature thermally modified fir-derived biomorphic C–SiC composites prepared by sol-gel infiltration, *Ceramics International* (2022), doi: https://doi.org/10.1016/j.ceramint.2022.11.119.

Ceramics International, Volume 49, Issue 6, March 2023, pp. 9523-9533
DOI:10.1016/j.ceramint.2022.11.119

Low-temperature thermally modified fir-derived biomorphic C-SiC composites prepared by sol-gel infiltration

Guo-Qing Li[1], Min Yu[1,*], Luo Hang[2], Ze-Ya Huang[1], Ren-Li Fu[1], Francesco Gucci[3], Theo Saunders[4], Kong-Jun Zhu[5], Dou Zhang[2]

[1] College of Materials Science and Technology, Nanjing University of Aeronautics and Astronautics, Nanjing 211106, China

[2] State Key Laboratory of Powder Metallurgy, Central South University, Changsha, China

[3] Surface Engineering and Precision Institute, Cranfield University, Bedfordshire MK430AL, UK

[4] School of Engineering and Materials Science, Queen Mary University of London, London, E1 4NS, UK

[5] College of Aerospace Engineering, Nanjing University of Aeronautics and Astronautics, Nanjing 211106, China

Abstract: In order to solve the problems (i.e. low infiltration efficiency, cracks, interface separation and poor mechanical properties) in the process of wood-derived C-SiC composites, the thermal modification of fir at low temperatures (300 ℃ ~ 350 ℃) combined with sol-gel infiltration was used to successfully produce biomorphic ceramics. The prepared materials were comprehensively characterized and exhibited improved interfacial bonding between C and SiC and mechanical properties. The weight gain per unit volume (0.123 g/cm^3) of SiO_2 gel in the fir thermally modified at 300 ℃ is 167.4 %, higher than that (0.046 g/cm^3) of the unmodified fir. A well-bonded interface was formed between the SiO_2 gel and the pore wall of the fir thermally modified at 300 ℃. With the increase of modification temperature from 300 ℃ to 350 ℃, the distance between SiO_2 gel and the pore wall increases, and a gap (1~3 μm) is observed between SiO_2 gel and the pore wall of the fir carbonized at 600 ℃. The C-SiC composites sintered at 1400 ℃ exhibited the highest compressive strength and bending strength of 40.8 ± 5.8 MPa and 11.7 ± 2.1 MPa, respectively, owing to the well-bonded interface between C of fir thermally modified at 300 ℃ and SiC. However, the composites sintered at 1600 ℃ for 120 min exhibited the lowest compressive

* Corresponding author: Min Yu
College of Materials Science and Technology,
Nanjing University of Aeronautics and Astronautics, Nanjing 211106, China
E-mail: min.yu@nuaa.edu.cn

strength and bending strength of 28.1 ± 13.4 MPa and 5.7 ± 1.6 MPa, respectively, which are 31.1 % and 51.3 % lower than those sintered at 1400 ℃ for 120 min, respectively. This might result from the porous structure formed by the excessive consumption of fir-derived carbon during the reaction between C and SiO_2 at 1600 ℃ for 120 min. Therefore, thermal modification in the preparation of biomorphic C-SiC composites can promote slurry infiltration and the formation of a well-bonded interface between C and SiC, thus improving the mechanical properties of the composites.

Keywords: thermally modified fir, Sol-gel, composites, compressive strength, bending strength

1. Introduction

Using a biochar template for producing wood-derived ceramics is promising for producing complex-shaped high-temperature ceramic components, owing to the excellent complex-shape capability and low cost of wood [1-4]. The biomorphic SiC composites have exhibited low-density, complex shape capability, remarkable wear resistance and excellent corrosion resistance, which are suitable for filters, supercapacitors and high-temperature components for aircraft [5, 6].

So far, several kinds of wood have been explored for the preparation of biomorphic SiC composites, including pine [7], oak [8], birch [9], balsa [10], beech [11], sipomahogany [12], iroko [13], shaddock peel [14] and so on. However, the resins and essential oils of wood can prevent the infiltration of the second material into its complex structure. The method of extracting resins from wood in a Soxhlet extraction apparatus for 24 h has been explored to solve this problem. However, this method is time-consuming and cannot be used to prepare large-volume bulk composites, and petroleum ether in the Soxhlet extractor is harmful to both environment and health [7]. The method of thermally modifying wood at low temperatures (300 ℃ ~ 350 ℃) has great potential to partially decompose the resins from the wood, and has barely been reported to be used for producing wood-derived ceramics. The thermal modification of wood is beneficial for introducing other materials (such as SiO_2 sol, PCS, etc.) into the wood-derived pore structure, owing to the enlarged pores and the excellent wettability between the infiltrated raw material and plant cell wall [7].

Several technologies have been developed to prepare biomorphic SiC composites, including melt infiltration (MI), chemical vapor infiltration (CVI), molten salt infiltration (MSI), sol-gel infiltration (Sol-gel), slurry infiltration (SI) and polymer precursor infiltration (PPI) [6, 13, 15-19]. Compared with the above methods, the sol-gel infiltration method has some advantages including lower material costs, a simpler production process, and the ability to maintain the structure and morphology of the initial template integrally [20, 21]. The mechanical properties of biomorphic SiC composites prepared by MI have been reported, while those produced by CVI, Sol-gel and SI have barely been reported, probably owing to the inhomogeneous microstructure [7, 11, 13, 16, 20, 22-25].

In the preparation of biomorphic C-SiC composites by sol-gel method, the infiltration of SiO_2 sol into the wood requires 5 repeated steps, and each step lasts at least 9h [10, 11]. However, the use of thermally-modified fir as a template can shorten the infiltration time (~10 min), and improve the interface bonding between SiO_2 gel and template after drying. Using fir as raw materials for preparing C-SiC composites has both considerable economic benefits and complex shape capability. This study investigates the effect of thermal modification temperatures (300 ℃, 325 ℃, 350 ℃) of fir on the template structure and the interface between the thermal-modified fir and SiO_2 gel in composites. In addition, this study investigates the effect of sintering temperature on the crystalline phase, microstructure, compressive strength and bending strength of the composites.

2. Experimental procedure

2.1 Material preparation

Fir (Jurong, Jiangsu Province) was dried at 80 ℃ for 24 h and then cut into rectangular specimens measuring approximately 25 mm (L) × 7 mm (T) × 7 mm (R). The shaped fir specimens were modified by the heat treatment in a nitrogen atmosphere at 300 ℃, 325 ℃, 350 ℃ and 600 ℃ for 40 min respectively. The geometric density of the fir before and after thermal modification was measured. Seven groups of SiO_2 precursor sol were formulated by mixing Tetraethyl Orthosilicate, ethanol, deionized water and concentrated hydrochloric acid (the molar ratio: 1: x: 2: 0.0484; x = 0.25, 0.5,

0.75, 1, 1.25, 1.5, 1.75). The viscosity of the SiO_2 sol was measured after stirring at 40 ℃ for 30min. The thermally modified fir was infiltrated with SiO_2 sol in a vacuum for 5 min. The infiltrated samples were dried in an oven at 60 ℃ for 12 hours. The preforms were repeatedly infiltrated 4 times by SiO_2 sol in a vacuum for 5 min. The samples were subsequently sintered at 1200 ℃, 1400 ℃ and 1600 ℃ for 120min in a tube furnace in an argon atmosphere. Fig. 1 shows the process of preparing the fir-derived C-SiC composites by sol-gel infiltration.

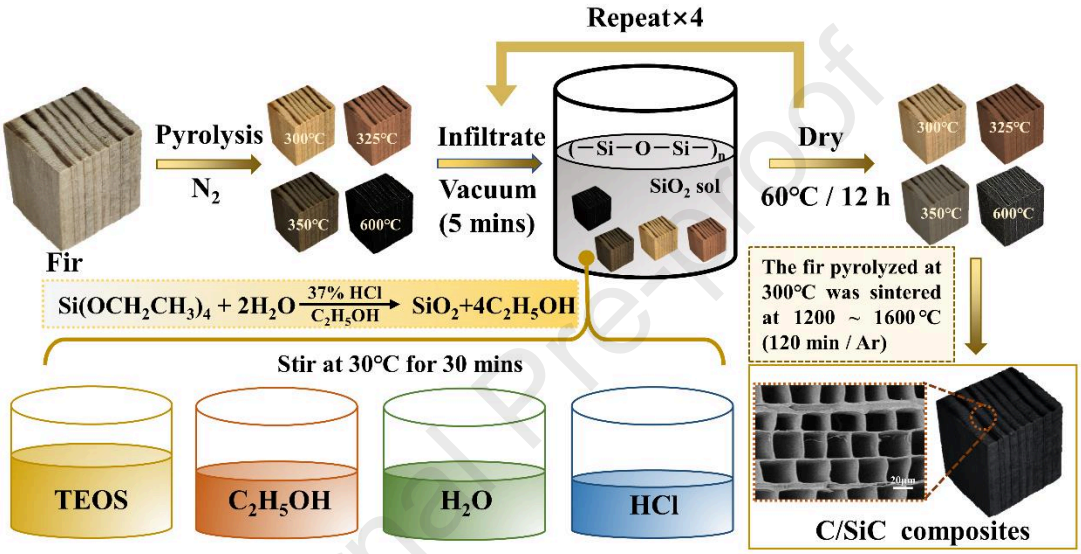

Fig. 1 The process of preparing the fir-derived C-SiC composites by sol-gel infiltration.

2.2 Characterization

Thermogravimetric analysis (TGA) was used to determine the weight loss during the heat treatment (100 ℃ ~ 1000 ℃) with a heating rate of 5 ℃/min in flowing N_2. Inspect-F scanning electron microscope (SEM, Hillsboro, OR) was used to investigate the microstructure of the samples. Digital viscometer (NDJ-9S, Bangxi Instrument Technology Co., LTD., Shanghai) was used to measure the viscosity of SiO_2 sol. X-ray powder diffraction apparatus (XRD, Malvern Panalytical-Empyrean ALPHA1, England) was used to detect the phases in the samples. A universal testing machine (Jinan metus testing technology-CMT5000 Co., LTD., China) was used to evaluate the mechanical properties of composites. Fourier transform infrared spectrometer (FTIR, Port East-850 Co., LTD, Tianjin) was used to detect the components of fir before and after thermal modification.

3. Results and discussions

3.1 Thermal modification and characterization of fir

Fig .2 shows the TG/DTG curves of fir at 50 ℃~ 600 ℃ in argon. The weight loss rate of the fir at 50 ℃ ~ 100 ℃ is ~5 %, owing to the loss of absorbed water, structure water and tar in the fir [26]. The weight loss of the fir at 200 ~ 400 ℃ reached the highest value of 65 %, mainly owing to the decomposition of cellulose, hemicellulose and lignin [27, 28]. Some small molecules (such as CO_2, fatty acids, carbonyls, and alcohols) evaporated from the fir at 200 ℃~ 400 ℃ [29]. The thermal modification was finished at 400 ℃, and a small weight loss (~3 %) of the fir is observed with the temperature rising further, owing to the decreases of the oxygen and hydrogen in the fir [7]. Based on the TG/DTG curve of the fir, the heating profile for thermal modification of the fir was optimized to shorten the processing time and reduce microcracks (Fig. 2b). The heating rates of 3 ℃/min and 5 ℃/min were set in the temperature range from 50 ℃ to 200 ℃ and from 400 ℃ to 600 ℃, respectively, owing to the slow weight loss. Tar and water in the fir were removed after thermal modification at 200 ℃ for 20 min. A slow heating rate of 1 ℃/min was set in the temperature range from 200 ℃ to the thermal modification temperature (300 ℃, 325 ℃, 350 ℃), owing to the rapid weight loss, at this stage small molecular gases (H_2, CH_4, H_2O, etc.) were released from the fir thermally modified at 300 ℃, 325 ℃ and 350 ℃ for 40 min. In addition, other firs were carbonized at 600 ℃ for 120 min. And finally, the samples were cooled by furnace cooling.

Fig .2c shows the images of the fir thermally modified at 300 ℃, 325 ℃, 350 ℃ and carbonized at 600 ℃. Different volume of cracks are observed in the fir thermally modified at 300 ℃, 325 ℃, 350 ℃ and carbonized at 600 ℃. A tiny crack is observed at 300 ℃ (marked in red dot circle in Fig.2c), a coarse crack is observed at 325 ℃, and more cracks are observed at 350 ℃ (about three cracks) and 600 ℃ (about five cracks). The formed cracks results from the rapid shrinkage of fir caused by both the evaporation of water and the decomposition of cellulose, hemicellulose and lignin. Therefore, the fir thermally modified at 300 ℃ was used as a template before infiltration. As shown

in Fig .2d, a self-made fixture (assembled by springs and metal sheets) was used to prevent the rapid evaporation of water in the fir to successfully reduce cracks [30].

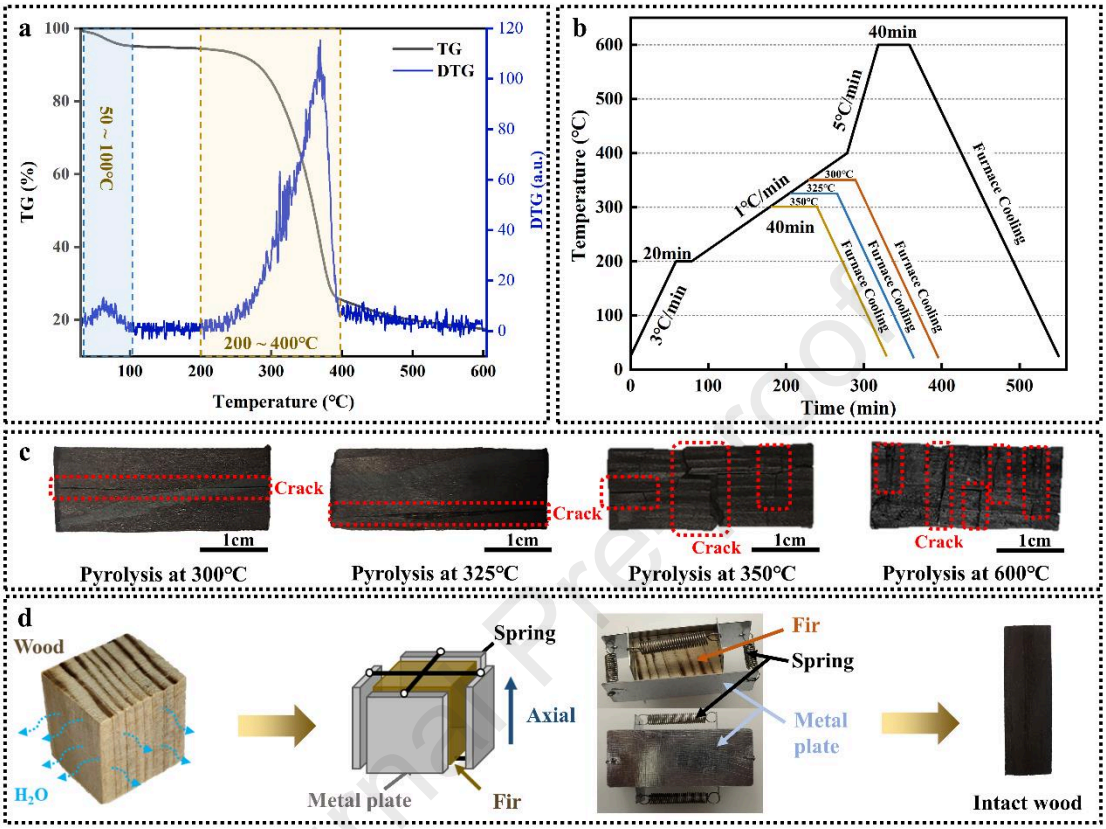

Fig. 2 (a) TG and DTG curves of the fir. (b) Thermal modification and pyrolysis profiles of the fir. (c) Images of the fir thermally modified at 300 ℃, 325 ℃, 350 ℃ and carbonized at 600 ℃. (d) A self-made fixture for the thermal modification to reduce cracks in the fir.

3.2 Effect of thermal modification temperature on the microstructures and compositions of fir

Fig. 3a-d shows the SEM micrographs of fir thermally modified at 300 ℃, 325 ℃, 350 ℃ and carbonized at 600 ℃. The complete pipeline structure can be observed in the fir thermally modified at 300 ℃, with the aid of self-made fixture. The pipeline structure of the fir was damaged by the increasing thermal modification temperature from 325 ℃ to 600 ℃. Loose structures are observed in the fir thermally modified at

325 ℃, some small cracks are observed in the fir thermally modified at 350 ℃, and a large number of cracks are observed in the fir carbonized at 600 ℃.

Fig. 3e shows the FTIR results of fir before and after thermal modification at 300 ℃, 325 ℃ and 350 ℃. The peak at 1033 cm^{-1} is the vibration of aromatic C-H and the vibration of C-O in primary alcohol. The peak intensity of fir thermally modified at 300 ℃ increased by 60.5 %, owing to the decomposition of C-O-C in cellulose and hemicellulose. The peak intensity of fir thermally modified at 325 ℃ and 350 ℃ decreased by 66.7 % and 92.7 %, respectively, owing to the decrease of primary alcohol above 325 ℃. The peak at 1159 cm^{-1} is the stretching vibration of C-O in phenol. The peak intensity of fir thermally modified at 300 ℃ increased by 51.2 %, owing to the destruction of aromatic ether bonds in lignin and the formation of phenolic hydroxyl groups. The peak intensity of fir thermally modified at 325 ℃ and 350 ℃ decreased by 58.1 % and 97.1 %, respectively, owing to the reduction of phenolic hydroxyl groups during thermal modification at 325 ℃ and 350 ℃. The peaks at 1429 cm^{-1}, 1464 cm^{-1}, 1509 cm^{-1} and 1601 cm^{-1} are C-H stretching vibrations. These peaks are weak above 325 ℃, owing to the release of C-H transformed small molecules (such as CH_4 and H_2). The peak at 2937 cm^{-1} is the stretching vibration of C-H in methyl and methylene groups. The peak intensity of the fir thermally modified at 300 ℃ increased by 145 %, owing to the increase of methyl and methylene generated by the decomposition of cellulose, hemicellulose and lignin. The peak at 3408 cm^{-1} is the stretching vibration of O-H. The peak intensity of the fir thermally modified at 300 ℃ increased by 135.5 %, owing to the decomposition of C-O-C in cellulose and hemicellulose and the formation of alcohols. The peak intensity of fir thermally modified at 325 ℃ and 350 ℃ decreased by 48.4 % and 69.9 %, respectively, owing to the reduction of alcohols above 325 ℃.

Fig. 3f and g show the shrinkage (length, width and height) and the weight loss ratio of fir before and after thermal modification at 300 ℃, 325 ℃, 350 ℃ and carbonization at 600 ℃. The shrinkage and the weight loss rate of the fir increase with the increased thermal modification temperature from 300 ℃ to 600 ℃, owing to the ~~thermal modification~~ partial decomposition of the main components (such as cellulose,

hemicellulose and lignin) of the fir. Fig. 3h shows the density of the fir before and after thermal modification at 300 ℃, 325 ℃, 350 ℃ and carbonization at 600 ℃. The fir thermally modified at 325 ℃exhibited highest density of 0.36 g/cm^3,, owing to its large shrinkage rate (6.0 % × 18.0 % × 30.1 %). The fir thermally modified at 300℃ exhibited relatively lower density of 0.32 g/cm^3, owing to the relatively smaller shrinkage of fir.

To sum up, the mechanism of thermal modification of fir is the decomposition of macromolecules (i.e. cellulose, hemicellulose and lignin) into monomers (i.e. volatile phenolic hydroxyl and alcohol hydroxyl) by heating above 300 ℃, owing to the destruction of the C-O-C, C-H and O-H bonds in the fir. The higher thermal modification temperatures (300 ~ 350 ℃) result in the greater shrinkage rate and weight loss rate of fir. The density of the thermally modified fir is affected by both the shrinkage rate and weight loss rate.

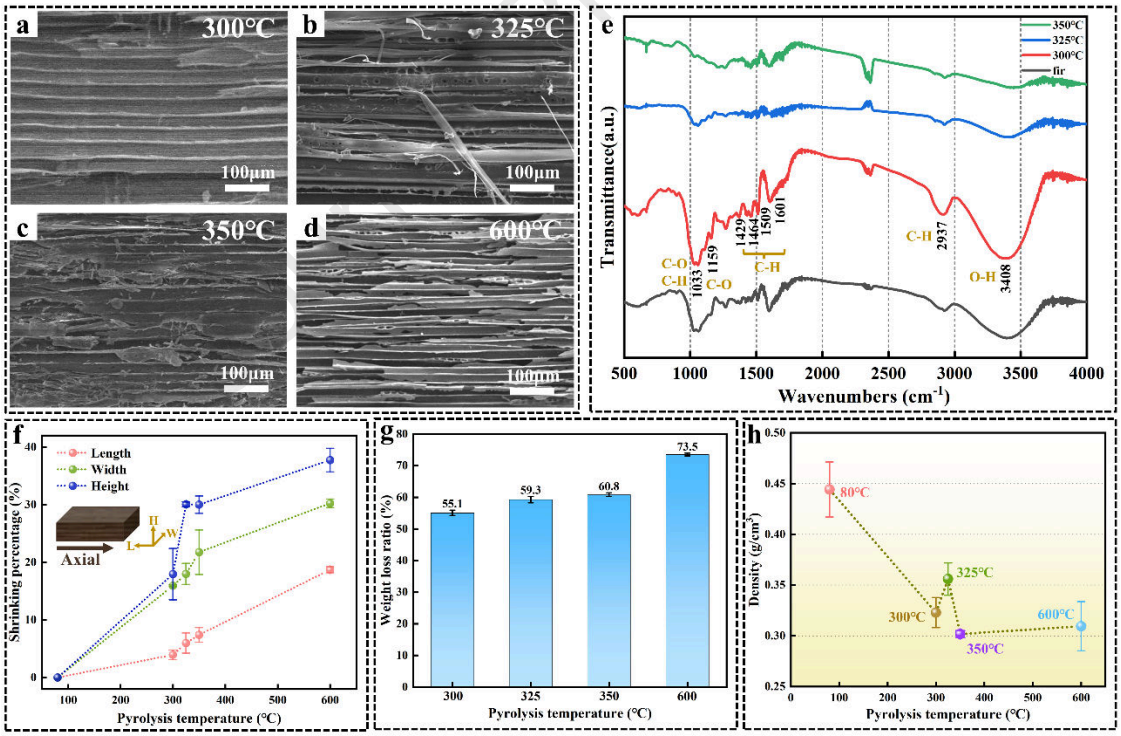

Fig. 3 SEM micrographs of fir thermally modified at 300 ℃ (a), 325 ℃ (b), 350 ℃ (c) and carbonized at 600 ℃ (d). (e)FTIR of fir before and after thermal modification at 300 ℃, 325 ℃ and 350 ℃. Shrinkage of length, width and height (f), weight loss rate (g) and density (h) of fir before

and after thermal modification at 300 ℃, 325 ℃, 350 ℃ and carbonization at 600 ℃.

3.3 Effect of thermal modification temperature of fir on the infiltration of SiO_2 sol

Fig. 4a shows the viscosity of SiO_2 sol prepared by different molar ratios (x:1, x = 0.25, 0.5, 0.75, 1, 1.25, 1.5, 1.75) of ethanol and tetraethyl orthosilicate (TEOS). When x is between 0.25 and 1, the viscosity of SiO_2 sol decreases with the decrease of TEOS content, but when x is between 1 and 1.8, the viscosity of SiO_2 sol almost remains unchanged. The SiO_2 sol with the molar ratio of ethanol to TEOS of 1:1 has both high silicon content and low viscosity. Therefore, the SiO_2 sol with the molar ratio of ethanol to TEOS of 1:1 was chosen to be infiltrated into the fir to produce biomorphic ceramics. Fig. 4b, c and d show the weight gain rate, density and the increased weight per unit volume of the fir (thermally modified at 300 ℃, 325 ℃, 350 ℃ and carbonized at 600 ℃) after different times (1, 2, 3 and 4) of infiltration. It can be observed that the fir thermally modified at 300 ℃ is characterized by low density after infiltration. Compared with the unmodified fir, SiO_2 sol was easier to infiltrate into the fir thermally modified at 300 ℃, resulting in the higher weight gain rate of fir modified at 300 ℃. However, compared with the fir thermally modified at 300 ℃, SiO_2 sol was easier to infiltrate into the fir thermally modified at 325 ℃ or above, resulting in the higher weight gain rate of fir modified at 325 ℃ or above.-Fig. 4e shows the optical images of fir (thermally modified at 300 ℃)-SiO_2 gel composites. The SiO_2 gels infiltrated into fir thermally modified at 300 ℃ can be observed in the images of the composite.

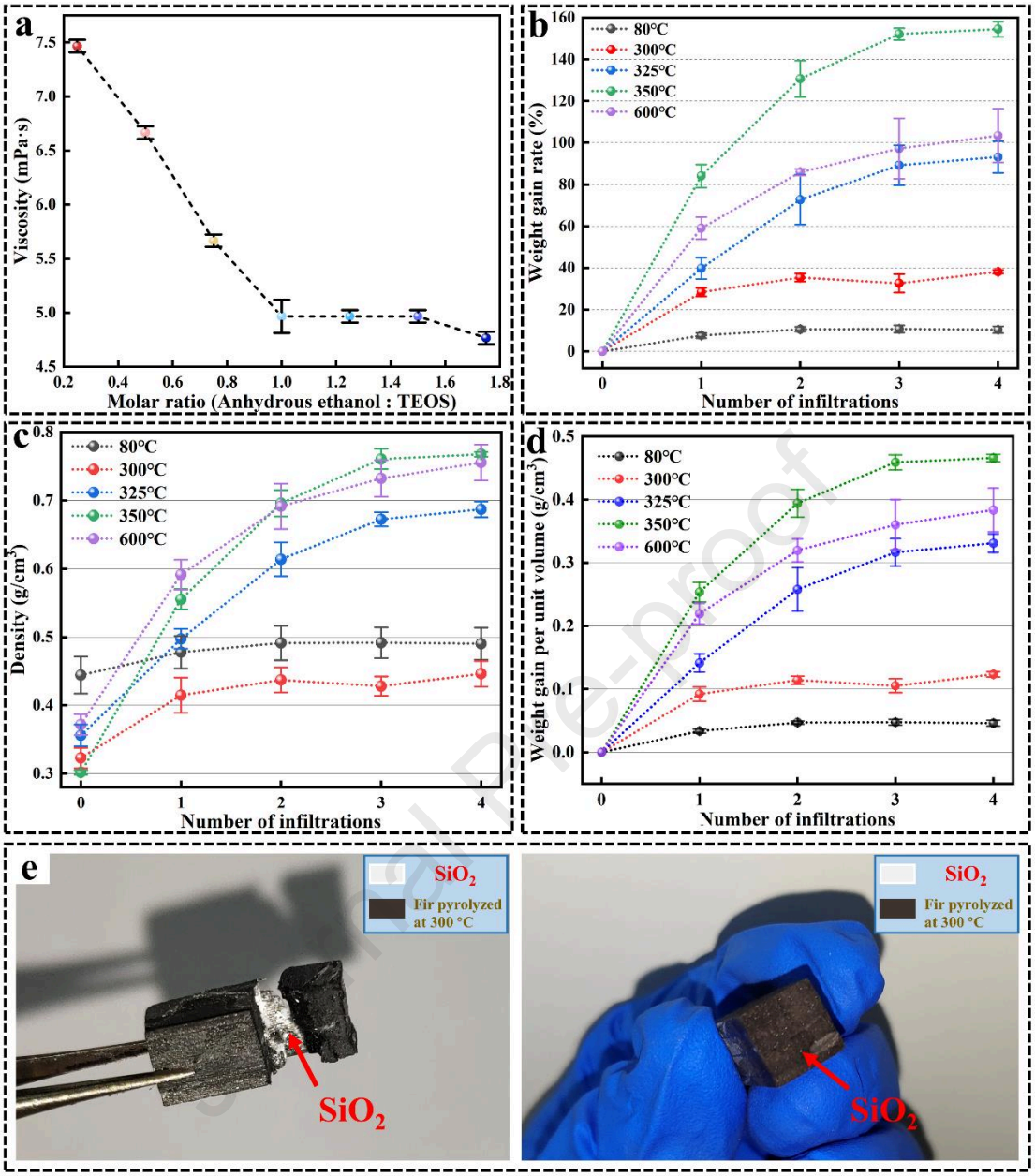

Fig. 4 (a) The viscosity of SiO_2 sol with the molar ratio of orthosilicate and ethanol (1:x, x = 0.25, 0.5, 0.75, 1, 1.25, 1.5, 1.75). Weight gain rate(b), density (c) and the increased weight per unit volume (d) of the fir (thermally modified at 300 ℃, 325 ℃, 350 ℃ and carbonized at 600 ℃) after different times (1, 2, 3 and 4 times) of infiltration. (e) The images of the thermally modified fir (at 300 ℃)-SiO_2 gel composites.

Fig. 5a-h shows the SEM micrographs of thermally-modified fir-SiO_2 gel composites. As shown in Fig. 5b, d, f and h, the higher thermal modification temperatures of fir result in the weaker interface bond between SiO_2 gel and pore wall,

which were clarified in Fig.5 i-l. The fir thermally modified at 300 ℃ exhibits the well-bonded interfaces between pore wall and SiO_2 gel in Fig.5 a and b, owing to the hydrogen bonding between the organic components (such as cellulose, hemicellulose and lignin) left by the incomplete decomposition of the fir and SiO_2 gel (as shown in Fig. 5i). Fig. 5a-h shows the damage degree of pore wall increases with the increased thermal modification temperature of the fir (damage areas are marked in red dot circle in Fig.5e and g). The damage of original pore wall in the fir probably results from the decomposition of the main components (cellulose, hemicellulose and lignin).

To sum up, the thermal modification at 300 ℃, 325 ℃, 350 ℃ and carbonization at 600 ℃ improves the infiltration efficiency of SiO_2 gel into the fir, compared with unmodified fir. The fir thermally modified at 300 ℃ should be selected as an infiltration template, owing to its intact pipe structure and fewer cracks than the fir thermally modified above 325 ℃ (as shown in Fig. 3a-d). In addition, the thermal modification at 300 ℃ leads to the well-bonded interfaces between SiO_2 gels and the fir.

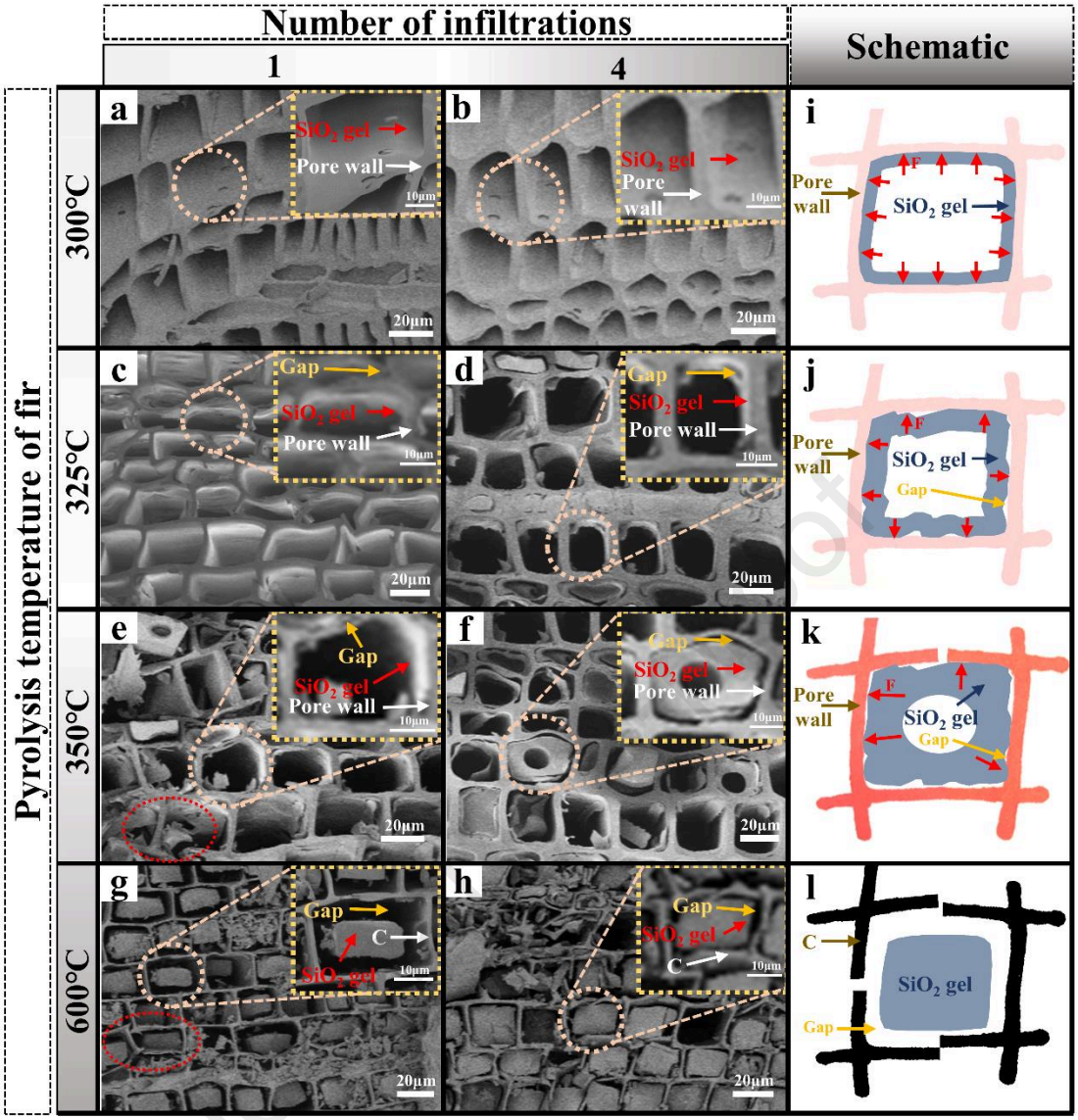

Fig. 5 SEM micrographs of the thermally-modified fir-SiO_2 gel composites: (a) fir (thermally modified at 300 ℃)-SiO_2 (1 time of infiltration), (b) fir (thermally modified at 300 ℃)-SiO_2 (4 times of infiltration), (c) fir (thermally modified at 325 ℃)-SiO_2 (1 time of infiltration), (d) fir (thermally modified at 325 ℃)-SiO_2 (4 times of infiltration), (e) fir (thermally modified at 350 ℃)-SiO_2 (1 time of infiltration), (f) fir (thermally modified at 350 ℃)-SiO_2 (4 times of infiltration), (g) fir (carbonized at 600 ℃)-SiO_2 (1 time of infiltration), (h) fir (carbonized at 600 ℃)-SiO_2 (4 times of infiltration). Schematic of infiltration of SiO_2 sol in fir thermally modified at 300 ℃ (i), 325 ℃ (j), 350 ℃ (k) and carbonized at 600 ℃ (l).

3.4 Effect of sintering temperature on phases and microstructures of the fir-derived ceramics

Fig. 6a shows the heating profile of the thermally-modified fir-SiO_2 gel composites. The heating rate from room temperature to 300 ℃ and from 400 ℃ to sintering temperature (1200 ℃, 1400 ℃ and 1600 ℃) was set at 5 ℃/min. The heating rate from 300 ℃ to 400 ℃ was set at 2 ℃/min, and the holding time at 400 ℃ was set at 30 min, in order to slowly release the gas of decomposition of organic components in the fir. The sintering time was 120 min to make the carbon and SiO_2 react completely. The cooling rate from sintering temperature (1200 ℃, 1400 ℃ and 1600 ℃) to 800 ℃ was set at 2 ℃/min to prevent cracks caused by the rapid temperature reduction and the sample was cooled by furnace cooling below 800 ℃. Fig. 6b shows the images and XRD patterns of the composites sintered at 1200 ℃, 1400 ℃ and 1600 ℃, respectively. Almost no macroscopic cracks are observed on the surface of the composites. Some gray areas are observed on the surface of the fir-derived C-SiC composites sintered at 1600 ℃, owing to the excessive consumption of carbon in the reaction with SiO_2 (as shown in supplementary Fig. S2).

As shown in Fig. 6b, the broad peak at $2\theta = 21.5°$ correspond to the amorphous carbon and amorphous SiO_2. The broad peak at $2\theta = 21.6°$ corresponds to the amorphous carbon. The sharp peaks at $2\theta = 35.7°$, $2\theta = 60.1°$ and $2\theta = 72.0°$ correspond to the (111), (220) and (311) crystal planes of the SiC. The sharp peaks at $2\theta = 43.9°$ and $2\theta = 75.3°$ correspond to the (111) and (220) crystal planes of carbon. The peak of amorphous C and amorphous SiO_2 are observed in the composite sintered at 1200 ℃, indicating that carbon and SiO_2 cannot react to form silicon carbide at 1200 ℃. The peaks of SiC and amorphous carbon are observed in the composites sintered at 1400 ℃, indicating that carbon has reacted with SiO_2 at 1400 ℃ to form silicon carbide with good crystallinity. The peaks of SiC and carbon are observed in the composites sintered at 1600 ℃, indicating that carbon has reacted with SiO_2 at 1600 ℃ to form silicon carbide with excellent crystallinity.

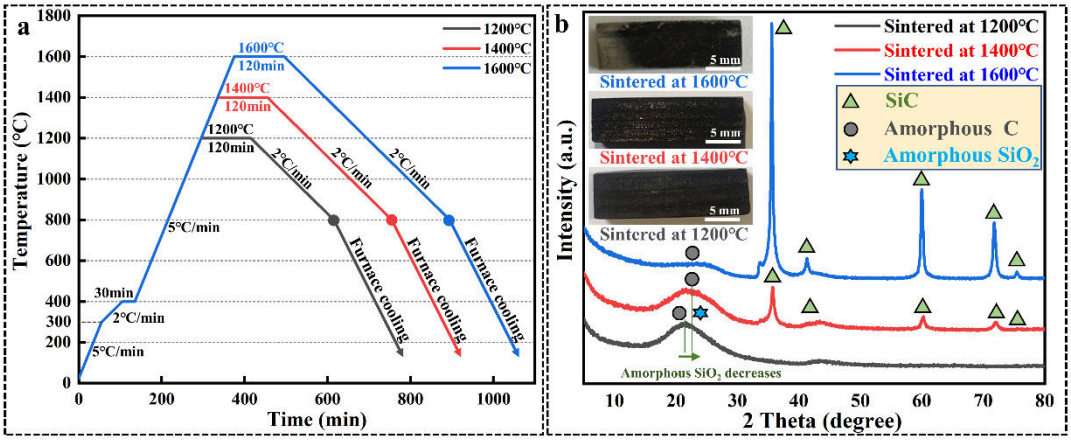

Fig. 6 (a) Heating profile of the thermal-modified fir-SiO_2 gel composites. (b) XRD patterns of the biomorphic composites sintered at 1200 ℃, 1400 ℃ and 1600 ℃. The insets are the optical photograph of corresponding composites.

Fig. 7a-c shows the SEM micrographs of the fir-derived composites sintered at 1200 ℃, 1400 ℃ and 1600 ℃. The complete pore structure of the fir and a small amount of silk (probably from the fir carbon) in the pores are observed in the composites sintered at 1200 ℃ (as shown in Fig. 7a and the red dot circle in Fig. 7a_1). Thin carbon pore walls, small additional pores (as shown in the yellow dot circle in Fig. 7b_1) on the pore wall and many ribbons (probably from the fir carbon) in the pores are observed in composites sintered at 1400 ℃ (as shown in Fig. 7b and the red dot circle in Fig. 7b_1). SiC grains arranged closely on the pore wall are observed in the composites sintered at 1600 ℃, as well as well-bonded interfaces between the carbon layer and the SiC layer (as shown in Fig. 7c and Fig. 7c_1 and c_2), owing to the good wettability between the fir thermally modified at 300 ℃ and the SiO_2 gel. Fig. 7d shows the schematic of the reaction mechanism between the fir thermally modified at 300 ℃ and SiO_2 gel. The fir thermally modified at 300 ℃ was completely carbonized above 600 ℃, and SiO_2 gel was converted into amorphous SiO_2, which reacts with carbon at high temperatures (>1400 ℃) to form SiC [31].

Fig. 7e shows the sintering shrinkage and the density of the fir-derived composites sintered at 1200 ℃, 1400 ℃ and 1600 ℃. All the composites exhibit the similar

shrinkage (length: 22% ± 2%; height: 19% ± 2%; width: 18% ± 2%), and the shrinkage in the axial direction is greater than that in the radial direction, owing to the cellular pore structure. The density of the composites decreases from 0.92 g/cm^3 to 0.35 g/cm^3 with the increased sintering temperatures from 1200 ℃ to 1600 ℃. The composites sintered at 1400 ℃ exhibit the density of 0.67 g/cm^3.

Fig. 7f shows a summary of shrinkages (direction: L) and densities of biomorphic composites derived from natural materials. Compared with the shrinkage of ceramics derived from other natural materials (Birch [21]: 31.3 %, Oak [32]: 46.15 %, Coir [22]: 23.5 %), the shrinkage of the thermally-modified fir-derived composites sintered at 1200 ℃, 1400 ℃ and 1600 ℃ (22.6 %, 21.2 %, 22.6 %) is lower, and it is similar to the shrinkage (18.9 %) of extracted pine-derived ceramics [7, 20].

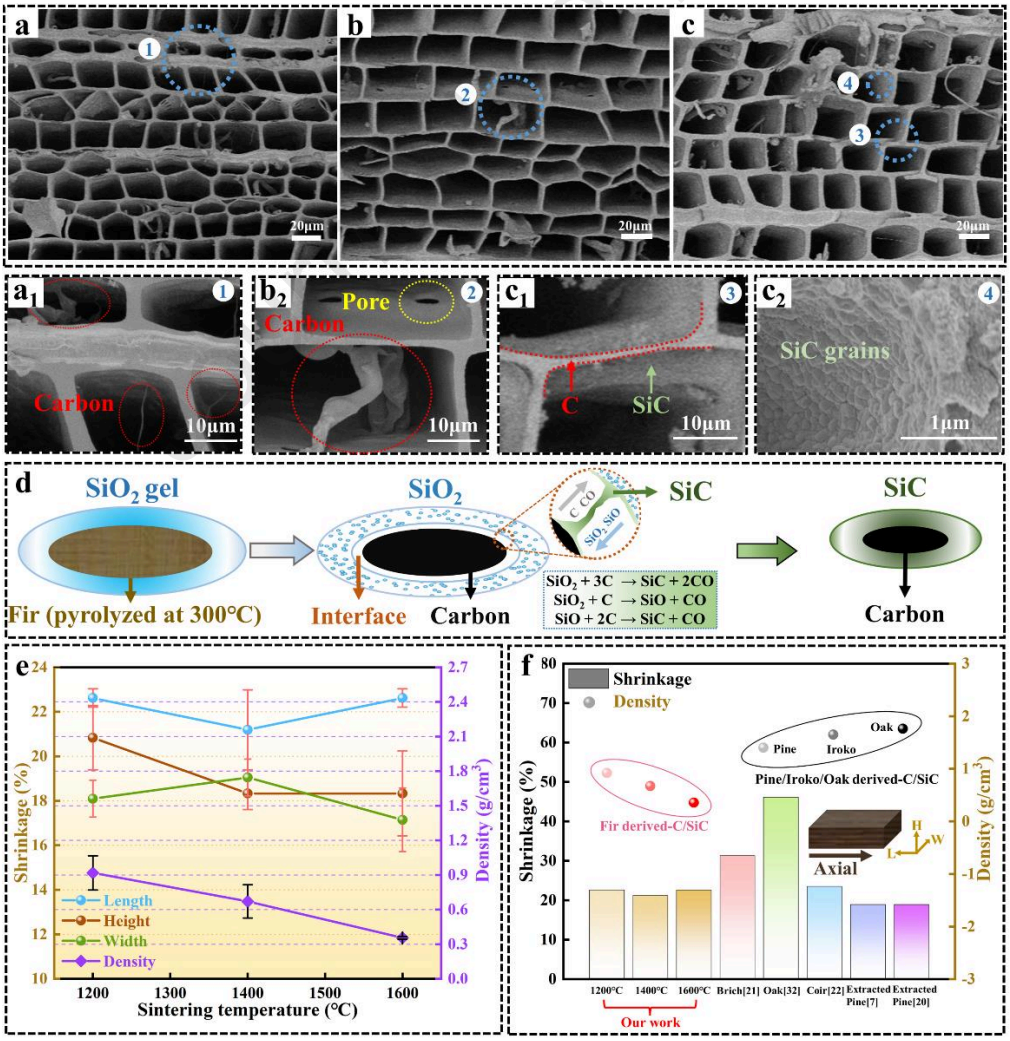

Fig. 7 SEM micrographs of the fir-derived composites sintered at 1200 ℃ (a), 1400 ℃ (b) and 1600 ℃ (c) (Fig. 7a_1, b_1, c_1 and c_2 correspond to positions 1, 2, 3 and 4 in Fig. 7a, b and c, respectively). (d) Schematic of reaction mechanism between the fir thermally modified at 300 ℃ and SiO_2 gel. (e) Sintering shrinkage and density of the fir-derived composites sintered at 1200 ℃, 1400 ℃ and 1600 ℃. (f) Summary of shrinkage (direction: L) and density of biomorphic composites derived from natural materials.

3.5 Mechanical properties of the fir-derived composites

Fig. 8a shows the schematic of the compression test and bending test of the fir-derived composites, the parameters are shown in Fig. 8a. The compressive strength (P) and bending strength (R) are calculated by the following Eq. (1) and Eq. (2)

$$P = \frac{F_1}{S} \quad (1)$$

$$R = \frac{3 \cdot F_2 \cdot L}{2 \cdot b \cdot h^2} \quad (2)$$

Where P: compressive strength (MPa); F_1: destroy load in compression test (kN); S: stressed area (mm^2); R: bending strength (MPa); F_2: destroy load in bending test (kN); L: span (mm); b: width of sample (mm); h: height of sample (mm).

Fig. 8b and c show the force-displacement curves of compression tests and bending tests of the composites sintered at 1200 ℃, 1400 ℃ and 1600 ℃. The test curves all exhibit serrated shapes, owing to the brittleness of the porous C-SiC composite. Fig. 8d shows the compressive strength and bending strength of the fir-derived composites. The composites sintered at 1400 ℃ exhibit the highest compressive strength of 40.8 ± 5.8 MPa. The composites sintered at 1200 ℃ exhibit higher compressive strength of 39.7 ± 11.47 MPa, than that (28.1 ± 13.4 MPa) of the composites sintered at 1600 ℃. The composites sintered at 1200 ℃ exhibit the highest bending strength of 12.4 ± 0.7 MPa, owing to the infiltrated SiO_2 (as shown in Fig. 9i). The composites sintered at 1400 ℃ exhibit higher bending strength of 11.7 ± 2.1 MPa, than that (5.7 ± 1.6 MPa) of the composites sintered at 1600 ℃, owing to the homogeneous microstructures (as shown in Fig. 7d). Increasing the thermal modification time and the time of vacuum infiltration might be beneficial to decrease

the error bar of the mechanical properties in composites. Fig. 8d shows the large error of compressive strength and bending strength data, owing to the instability of the preparation process. The following aspects can be considered: 1. The thermal modification time of fir at 300 °C should be increased to increase the porosity of thermally modified fir; 2. The time of vacuum infiltration should be increased to make the SiO_2 sol infiltrate evenly.

Fig. 8e shows a summary of the compressive strength and bending strength of biomorphic composites derived from natural materials. The general range of the compressive/bending strength of charcoal is 1 ~ 10 MPa [33-35]. A. Gómez-Martín et al. prepared the pine-derived C-SiC composites and the iroko-derived C-SiC composites, and their compressive strength is increased by ~525 % and ~450 %, respectively, compared with that of the pine/iroko-charcoal [36]. However, the compressive strength of the fir-derived composites sintered at 1200 °C, 1400 °C and 1600 °C is increased by 892 %, 921 % and 602 %, respectively, compared with that of the fir-charcoal (~4 MPa). The outstanding compressive strength of the composites may result from the unreacted SiO_2 (as shown in Fig. 9a) and tightly packed SiC (as shown in the inset in Fig. 7c) as reinforcements in composites sintered at 1400 °C and 1600 °C. E. Vogli et al. and J. M. Qian et al. prepared the pine-derived C-SiC composites, and their bending strength increased by ~447 % and ~1307 % compared with that of the pine-charcoal, respectively [37, 38]. However, the bending strength of the fir-derived C-SiC composites sintered at 1200 °C, 1400 °C and 1600 °C is increased by 315 %, 289 % and 91 %, respectively, compared with that of the fir-charcoal (~3 MPa). The poor bending strength of the composites may be due to the unreacted carbon in some regions (as shown in supplementary Fig. S1), the micropores in pore walls resulting from the excessive consumption of carbon in the reaction with SiO_2 (as shown in supplementary Fig. S2), and the intergranular crack propagation in the bending test (as shown in supplementary Fig. S3).

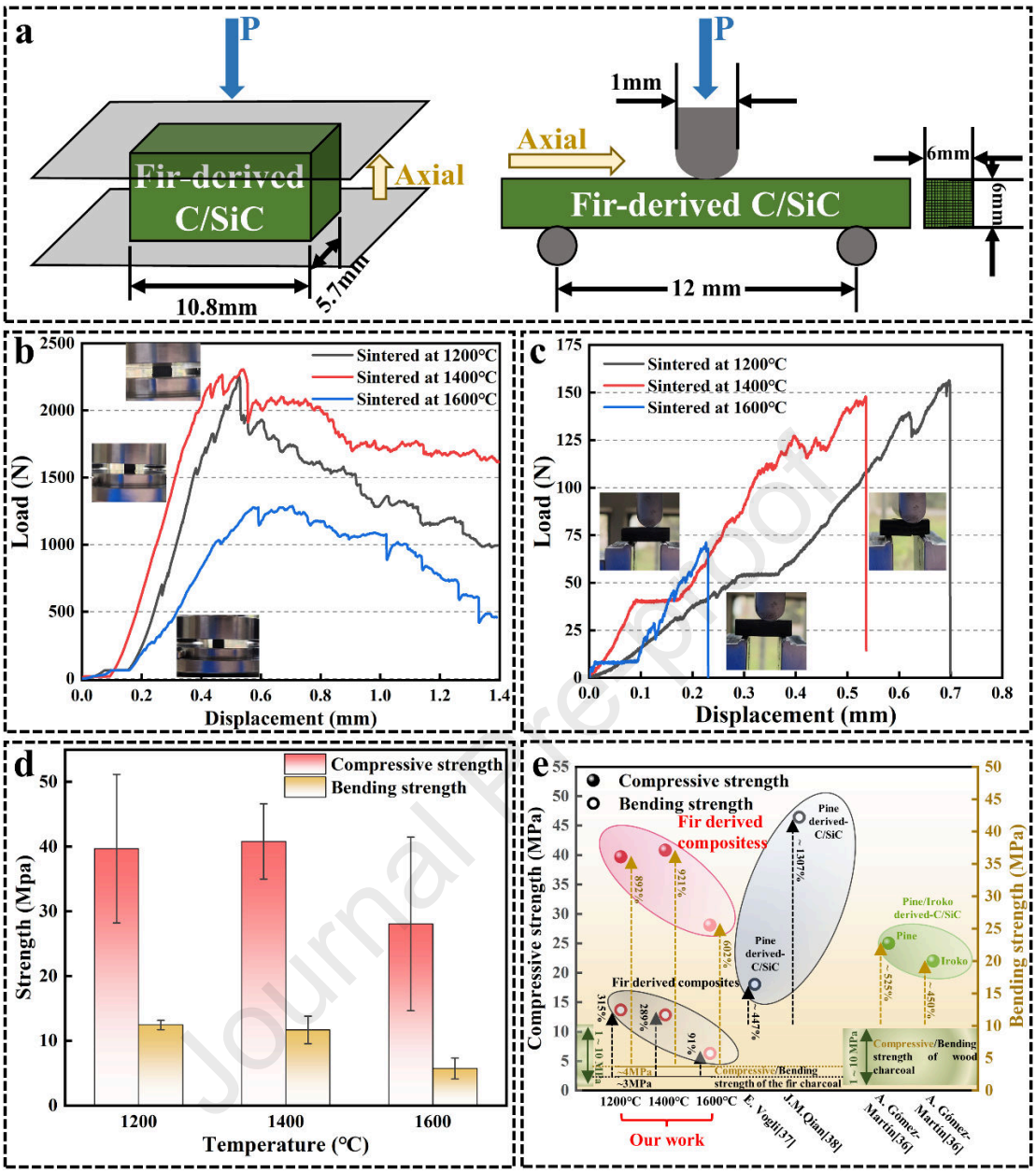

Fig. 8 (a) Schematic of compression test and bending test of the fir-derived composites sintered at 1200 ℃, 1400 ℃ and 1600 ℃. Force-displacement curves of compression tests (b) and bending tests (c) of the fir-derived composites sintered at 1200 ℃, 1400 ℃ and 1600 ℃. (d) Compressive strength and bending strength of the fir-derived composites sintered at 1200 ℃, 1400 ℃, and 1600 ℃. (e) Summary of compressive strength and bending strength of biomorphic composites derived from natural materials.

3.6 Cross-section analysis of the fir-derived composites

Fig. 9a-c shows the SEM micrographs of the cross-sections (after the bending test) of the fir-derived composites sintered at 1200 ℃, 1400 ℃ and 1600 ℃. Fig. 9d-e shows the images of crack shapes of the composites sintered at 1200 ℃, 1400 ℃ and 1600 ℃ after bending tests. Unreacted SiO_2 gel can be observed in the composites sintered at 1200 ℃. The crack shape of the composite is a step ladder (as shown in Fig. 9d), owing to the reinforcement of SiO_2 in the pores. A few filaments and thick pore walls can be observed in the composites sintered at 1400 ℃. The crack shape of the composite is oblique (as shown in Fig. 9e), owing to the inhomogeneity of the thickness of the pore wall. The crack shape of the composite sintered at 1600 ℃ is approximately linear (as shown in Fig. 9f), owing to the uniformity of the thickness of the pore wall and the brittleness of the composite.

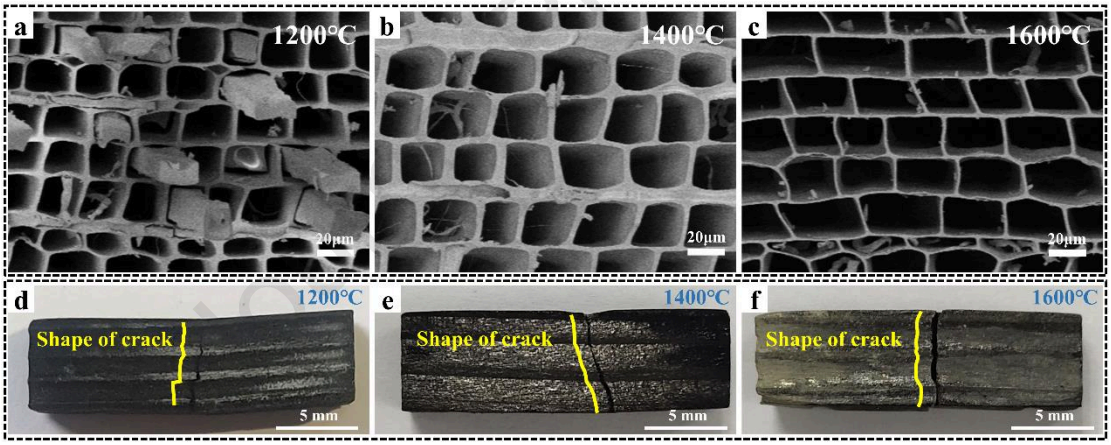

Fig. 9 SEM micrographs of the cross-sections (after the bending test) of the fir-derived composites sintered at 1200 ℃ (a), 1400 ℃ (b) and 1600 ℃ (c). The images of crack shapes of the composites sintered at 1200 ℃ (d), 1400 ℃ (e) and 1600 ℃ (f) after bending tests.

4. Conclusions

The low-temperature thermally-modified fir-SiO_2 gel-derived biomorphic C-SiC composites were successfully prepared. The higher thermal modification temperature (300 ℃ ~ 350 ℃) results in a larger gap between the SiO_2 gel and the pore wall. The

thermal modification temperature (300 ℃) of fir, induces few cracks and the good wettability between the fir and SiO_2 sol. Higher sintering temperatures (1400 ℃ ~ 1600 ℃) of the composites result in higher crystallinity of SiC, more reactions between C and SiO_2, and lower compressive strength and bending strength of the composites. The composites sintered at 1200 ℃ exhibit relatively high compressive strength (39.7 ± 11.47 MPa) and bending strength (12.4 ± 0.7 MPa), owing to the reinforcement of SiO_2. The composites sintered at 1400 ℃ exhibit relatively high compressive strength (40.8 ± 5.8 MPa) and bending strength (12.4 ± 0.7 MPa), owing to the generation of SiC phase. However, the compressive strength (28.1 ± 13.4 MPa) and bending strength (5.7 ± 1.6 MPa) of the composites sintered at 1600 ℃ are much lower than those sintered at 1400 ℃, owing to the excessive consumption of fir carbon in the reaction with SiO_2. Moreover, the composites sintered at 1400 ℃ exhibit a good bonding interface between C and SiC. The thermal modification of fir combined with sol-gel is promising in producing biomorphic C-SiC composites with homogenous microstructures and improved mechanical properties.

Acknowledgment

The authors gratefully acknowledge the support of Natural Science Foundation of Jiangsu Province (No. BK20200455), National Natural Science Foundation of China (No. 52002174), Innovation and entrepreneurship program of Jiangsu province, State Key Laboratory of Powder Metallurgy, Central South University, Changsha, China, and Innovation Project of Nanjing University of Aeronautics and Astronautics (xcxjh20210621).

Data availability statement

The data that support the findings of this study are available from the corresponding author upon reasonable request.

Appendix A. Supplementary data

Supplementary data related to this article can be found at xxx

References

[1] M. Yu, G.j. Zhang, T. Saunders, Wood-derived ultra-high temperature carbides and their composites: A review, Ceramics International, 46 (2020) 5536-5547.

[2] X.F. Wei, J.X. Liu, W.C. Bao, Y. Qin, F. Li, Y.C. Liang, F.F. Xu, G.J. Zhang, High-entropy carbide ceramics with refined microstructure and enhanced thermal conductivity by the addition of graphite, Journal of the European Ceramic Society, 41 (2021) 4747-4754.

[3] Y. Zeng, D. Wang, X. Xiong, X. Zhang, P.J. Withers, W. Sun, M. Smith, M. Bai, P. Xiao, Ablation-resistant carbide $Zr_{0.8}Ti_{0.2}C_{0.74}B_{0.26}$ for oxidizing environments up to 3000 ℃, Nature Communication, 8 (2017) 15836.

[4] D. Ni, Y. Cheng, J. Zhang, J.X. Liu, J. Zou, B. Chen, H. Wu, H. Li, S. Dong, J. Han, X. Zhang, Q. Fu, G.J. Zhang, Advances in ultra-high temperature ceramics, composites, and coatings, Journal of Advanced Ceramics, 11 (2021) 1-56.

[5] S. Zhang, X. Li, J. Zuo, J. Qin, K. Cheng, Y. Feng, W. Bao, Research progress on active thermal protection for hypersonic vehicles, Progress in Aerospace Sciences, 119 (2020) 100646.

[6] Q. Xu, X. Liu, Q. Luo, Y. Song, H. Wang, M. Chen, Y. Xuan, Y. Li, Y. Ding, Bifunctional biomorphic SiC ceramics embedded molten salts for ultrafast thermal and solar energy storage, Mater Today Energy, 21 (2021) 100764.

[7] J. Locs, L. Berzina-Cimdina, A. Zhurinsh, D. Loca, Optimized vacuum/pressure sol impregnation processing of wood for the synthesis of porous, biomorphic SiC ceramics, Journal of the European Ceramic Society, 29 (2009) 1513-1519.

[8] J.M. Qian, J.P. Wang, Z.H. Jin, Preparation of biomorphic SiC ceramic by carbothermal reduction of oak wood charcoal, Mat Sci Eng a-Struct, 371 (2004) 229-235.

[9] G.J. Qiao, Z.H. Jin, J.M. Qian, Biomorphic SiC ceramics prepared by organic template method, Key Eng Mat, 317-318 (2006) 167-172.

[10] H. Yamane, F. Kawamura, T. Yamada, Low-temperature synthesis of biomorphic cellular SiC ceramics from wood by using a Na flux, J Ceram Soc Jpn, 116 (2008) 163-165.

[11] U. Vogt, A. Herzog, T. Graule, R. Klinger, O. Paris, Wood derived SiC ceramics with oriented porous structures via carbothermal reduction [M], High Temperature Ceramic Matrix Composites, 2001, pp. 420-426.

[12] M.A. Bautista, J.Q. Cancapa, J.M. Fernandez, M.A. Rodríguez, M. Singh, Microstructural and mechanical evaluation of porous biomorphic silicon carbide for high temperature filtering applications, Journal of the European Ceramic Society, 31 (2011) 1325-1332.

[13] M.J. Lopez-Robledo, A. Gomez-Martin, J. Ramirez-Rico, J. Martinez-Fernandez, Sliding wear resistance of porous biomorphic sic ceramics, Int J Refract Met H, 59 (2016) 26-31.

[14] G.Q. Li, M. Yu, G.W. Lin, Y.L. Wang, L.X. Yang, J.X. Liu, F. Gucci, G.J. Zhang, Enhanced strength and thermal oxidation resistance of shaddock peel-polycarbosilane-derived C–SiC–SiO_2 composites, Ceramics International, https://doi.org/10.1016/j.ceramint.2022.06.045.

[15] C. Pflitsch, B. Curdts, B. Atakan, Atmospheric Pressure Chemical Vapor Infiltration (CVI) for the Preparation of Biomorphic SiC Ceramics Derived from Paper, J Nanosci Nanotechno, 11 (2011) 8416-8419.

[16] K.C. Hung, T.L. Wu, J.W. Xu, J.H. Wu, Preparation of Biomorphic Porous SiC Ceramics from Bamboo by Combining Sol-Gel Impregnation and Carbothermal Reduction, Polymers-Basel, 11 (2019) 1442.

[17] J.T. Zhu, F.L. Kwong, D.H.L. Ng, Synthesis of Biomorphic SiC Ceramic from Bamboo Charcoal, J Nanosci Nanotechno, 9 (2009) 1564-1567.

[18] L.Y. Wang, R.Y. Luo, G.Y. Cui, Z.F. Chen, Effects of pyrolysis temperatures on the oxidation behavior of PIP-processed SiCf/SiC composites, Ceramics International, 46 (2020) 17846-17856.

[19] Z. Yi, D. Wang, X. Xiang, Z. Xun, X. Ping, Ablation-resistant carbide $Zr_{0.8}Ti_{0.2}C_{0.74}B_{0.26}$ for oxidizing environments up to 3000 °C, Nature Communications, 8 (2017) 15836.
[20] A. Zhurinsh, J. Locs, L. Berzina-Cimdina, Investigation of the feasibility of pyrolytic obtaining of porous biomorphic SiC ceramics, J Anal Appl Pyrol, 85 (2009) 544-548.
[21] M. Adam, M. Oschatz, W. Nickel, S. Kaskel, Preparation of hierarchical porous biomorphic carbide-derived carbon by polycarbosilane impregnation of wood, Microporous & Mesoporous Materials, 210 (2015) 26-31.
[22] A. Maity, D. Kalita, N. Kayal, T. Goswami, O. Chakrabarti, P.G. Rao, Synthesis of biomorphic SiC ceramics from coir fibreboard preform, Ceramics International, 38 (2012) 6873-6881.
[23] V.V. Popov, T.S. Orlova, J. Ramirez-Rico, A.R. de Arellano-Lopez, J. Martinez-Fernandez, Electrical Properties of the SiC/Si Composite and the Biomorphic SiC Ceramic Fabricated from Spanish Beech Wood, Physics of the Solid State, 50 (2008) 1819-1825.
[24] T.E. Wilkes, M.L. Young, R.E. Sepulveda, D.C. Dunand, K.T. Faber, Composites by aluminum infiltration of porous silicon carbide derived from wood precursors, Scripta Materialia, 55 (2006) 1083-1086.
[25] V.V. Silberschmidt, Effect of material's randomness on scaling of crack Propagation in ceramics, International Journal of Fracture, 140 (2006) 73-85.
[26] T. Hosoya, H. Kawamoto, S. Saka, Cellulose–hemicellulose and cellulose–lignin interactions in wood pyrolysis at gasification temperature, J Anal Appl Pyrol, 80 (2007) 118-125.
[27] G. Liu, H. Song, J. Wu, Thermogravimetric study and kinetic analysis of dried industrial sludge pyrolysis, Waste Manag, 41 (2015) 128-133.
[28] S.I. Islamova, A.R. Khamatgalimov, Thermogravimetric and kinetic analyses of the thermal decomposition of fuel wood, Solid Fuel Chemistry, 51 (2017) 83-87.
[29] J.Y. Yeo, B.L.F. Chin, J.K. Tan, Y.S. Loh, Comparative studies on the pyrolysis of cellulose, hemicellulose, and lignin based on combined kinetics, Journal of the Energy Institute, 92 (2019) 27-37.
[30] S. Saft, M. Kaliske, A hybrid interface-element for the simulation of moisture-induced cracks in wood, Engineering Fracture Mechanics, 102 (2013) 32-50.
[31] H. Yoshino, K. Kamiya, H. Nasu, IR study on the structural evolution of sol-gel derived SiO_2 gels in the early stage of conversion to glasses, Journal of Non-Crystalline Solids, 126 (1990) 68-78.
[32] J. Li, S. Yu, M. Ge, X. Wei, Y. Qian, Y. zhou, W. Zhang, Fabrication and characterization of biomorphic cellular C/SiC–ZrC composite ceramics from wood, Ceramics International, 41 (2015) 7853-7859.
[33] N.W. Makgobelele, R.K.K. Mbaya, J.R. Bunt, N.T. Leokaoke, H.W.J.P. Neomagus, Evaluation of the mechanical properties of wood-derived charcoal briquettes for use as a reductant, Journal of the Southern African Institute of Mining and Metallurgy, 10.17159/2411-9717/903/2021.
[34] S.C. Das, S. Ashek-E-Khoda, M.A. Sayeed, Suruzzaman, D. Paul, S.A. Dhar, S.A. Grammatikos, On the use of wood charcoal filler to improve the properties of natural fiber reinforced polymer composites, Materials Today: Proceedings, 44 (2021) 926-929.
[35] A.M. Couto, T.C. Monteiro, P.F. Trugilho, J.T. Lima, J.R.M. da Silva, A. Napoli, D.P. de Almeida, Influence of physical-anatomical wood variables on charcoal physical–mechanical properties, Journal of Forestry Research, https://doi.org/10.1007/s11676-022-01462-9.
[36] A. Gomez-Martin, M.P. Orihuela, J.A. Becerra, J. Martinez-Fernandez, J. Ramirez-Rico, Permeability and mechanical integrity of porous biomorphic SiC ceramics for application as hot-gas filters, Materials & Design, 107 (2016) 450-460.

[37] E. Vogli, H. Sieber, P. Greil, Biomorphic SiC-ceramic prepared by Si-vapor phase infiltration of wood, Journal of the European Ceramic Society, 22 (2002) 2663-2668.
[38] J.M. Qian, Z.H. Jin, Preparation and characterization of porous, biomorphic SiC ceramic with hybrid pore structure, Journal of the European Ceramic Society, 26 (2006) 1311-1316.

Declaration of interests

☒ The authors declare that they have no known competing financial interests or personal relationships that could have appeared to influence the work reported in this paper.

☐The authors declare the following financial interests/personal relationships which may be considered as potential competing interests:

Low-temperature thermally modified fir-derived biomorphic C–SiC composites prepared by sol-gel infiltration

Li, Guo-Qing

2023-02-10

Li GQ, Yu M, Luo H, et al., (2023) Low-temperature thermally modified fir-derived biomorphic C–SiC composites prepared by sol-gel infiltration. Ceramics International, Volume 49, Issue 6, March 2023, pp. 9523-9533

https://doi.org/10.1016/j.ceramint.2022.11.119